

# Variations in dust-related PM<sub>10</sub> emission from an arid land due to surface composition and topsoil disturbance

Avraham Edri<sup>1</sup> · Avraham Dody<sup>2</sup> · Smadar Tanner<sup>1</sup> · Nitzan Swet<sup>1</sup> · Itzhak Katra<sup>1</sup>

Received: 27 May 2016 / Accepted: 18 August 2016 / Published online: 25 August 2016  
© Saudi Society for Geosciences 2016

**Abstract** Aeolian (wind) erosion is most common in arid regions. The resulted emission of PM<sub>10</sub> (particulate matter that is smaller than 10 μm in diameter) from the soil has many environmental and socioeconomic consequences such as soil degradation and air pollution. Topsoil resistance to aeolian transport highly depends on the surface composition. The study aim was to examine variations in PM<sub>10</sub> fluxes in a desert-dust source due to surface composition and topsoil disturbance. Aeolian field experiments using a boundary layer wind tunnel alongside soil composition analysis were integrated in this study. The results show variations in PM<sub>10</sub> fluxes (ranging from 9.5 to 524.6 mg m<sup>-2</sup> min<sup>-1</sup>) in the studied area. Higher wind velocity increased significantly the PM<sub>10</sub> fluxes in all surface compositions. A short-term natural disturbance caused changes in the aggregate soil distribution (ASD) and increased significantly PM<sub>10</sub> emissions. Considering that PM<sub>10</sub> contains clays, organic matter, and absorbed elements, the recorded PM<sub>10</sub> fluxes are indicative of the potential soil

loss and degradation by wind erosion in such resource-limited ecosystems. The findings have implications in modeling dust emission from a source area with complex surfaces.

**Keywords** Soil erosion · Sand flux · Aeolian processes · Soil loss · Dust source · Saltators

## Introduction

Aeolian (wind) soil erosion is a common process in arid regions that can lead to dust emission into the atmosphere. Dust emission has significant impacts on the Earth's systems depending on the physical and chemical characteristics of the topsoil (Shao, 2008). The emission of dust from soils is a major concern due to soil degradation by loss of clays (< 2 μm) and fine silt (< 10 μm), and absorbed nutrients. In addition, emission of PM<sub>10</sub> and PM<sub>2.5</sub> (particulate matter that is smaller than 10 and 2.5 μm in diameter, respectively) to the atmosphere increases air pollution and health risks particularly in arid environments (Ganor et al., 2009; Krasnov et al., 2014; Vodonos et al., 2014; Yitshak-Sade et al., 2015).

The surface characteristics determine the critical value (threshold) of wind (friction) velocity at which the aerodynamic drag is enough to dislodge particles from the surface and initiate their transport (Bagnold, 1941; Kok et al., 2012). Direct aerodynamic lifting is a dominant mechanism for loose fine-particle emission such as PM<sub>10</sub>. However, emission of cohesive fine particles (e.g., clays) is enabled only under higher wind velocities and/or under saltation flow (Bagnold, 1941; Kok et al., 2012). The presence of sand particles in the soil enables the entrainment of fine particles (clay and silt) by ballistic impact (saltation bombardment) (Shao et al., 1993). Surface cover such as vegetation and rock fragments increases surface roughness and thus reduces near-surface wind

✉ Itzhak Katra  
katra@bgu.ac.il

Avraham Edri  
polaedri@gmail.com

Avraham Dody  
dodik@post.bgu.ac.il

Smadar Tanner  
tanner@post.bgu.ac.il

Nitzan Swet  
swet@post.bgu.ac.il

<sup>1</sup> Department of Geography and Environmental Development, Ben Gurion University of the Negev, Be'er-Sheva, Israel

<sup>2</sup> Environmental Research Unit, Nuclear Research Center-Negev, Be'er-Sheva, Israel

velocities and erosion (Wolfe and Nickling, 1993; Gillies et al., 2006; Li et al., 2005). Crusted surface layer significantly reduces soil erodibility, where the strength of crusts varies with the composition and distribution of the binding media (Belnap and Gillette, 1998; Langston and McKenna Neuman 2005; Zaady et al., 2014). Among the soil properties, the dry aggregate size distribution of the topsoil is a major factor influencing the resistance to wind erosion. High proportion of erodible fraction (EF) (aggregates  $>840 \mu\text{m}$ ) in the upper layer of the soil surface increase its erodibility (Hevia et al., 2007; Van Pelt et al., 2013; Li et al., 2015; Swet and Ktra, 2016).

Desert environments are associated with a diverse range of geomorphological landforms such as desert pavements, playas, and alluvial fans that constitute source areas of dust emission (Bacon et al., 2011; Sweeney et al., 2011; Al-Dousari and Al-Awadhi 2012). The specific surface properties and the presence of different features on the surface (e.g., vegetation, crusts or rock fragments) control the magnitude of dust-related PM<sub>10</sub> emission from a specific soil (King and Nickling, 2005; Bacon et al., 2011; Hoffmann and Funk, 2015). It has been shown that topsoil disturbance can significantly accelerate aeolian erosion and PM<sub>10</sub> flux compared with natural (non-disturbed) crusted topsoil's (Sharratt et al., 2010; Baddock et al., 2011; Singh et al., 2012).

Soils in many deserts throughout the world are subjected to strain of increased human pressure and thus changes in their physico-chemical properties and potential of dust emission. The underlying assumptions about the surface complexity in a dust source incorporated into the dust emission models limit their accuracy. Knowledge about the variability of actual dust emission at various scales is still lacking. Ktra and Lancaster (2008) demonstrated spatio-temporal variability in the surface sediments of identified source area to reveal the potential changes for dust emissions over time. The study aim was to examine variations in PM<sub>10</sub> fluxes due to surface composition and topsoil disturbance. Aeolian field experiments by a boundary layer wind tunnel were applied to quantify the PM<sub>10</sub> fluxes from a study area with typical soil characteristics of arid dust sources.

## Material and methods

### Experimental plots

The study was conducted on desert soils of the Negev (Yamin Plain), Israel. The tested soils in Yamin Plain have not been exposed to anthropogenic activities as it is a part of natural reserves. The annual average rainfall is  $\sim 75$  mm. The silt-loam soils are characterized by low content of organic matter ( $< 1\%$ ) and a wide range of sand/clay percentage depending on the specific site location. During the majority of the year,

the topsoil is dry and is subjected to intensive aeolian erosion. The dominant wind direction is northwest during the day and alternates to southwestern along the night. The wind velocities can exceed up to  $13 \text{ m s}^{-1}$  (measured 6 m above the soil surface).

Experimental plots were designed within a closed area without human interference during the last six decades. The experimental plots for the soil sampling and the aeolian experiments (see below) were representative of the surface cover in the area (Fig. 1): an extensive coverage of mechanical crust (MC), sparse vegetation-shrubs cover (SV) with a typical distance of about 2 m between adjunct shrubs, and soil mechanical crust covered with different sizes (up to 15 cm in diameter) of rock fragments (RF).

### Soil analysis

In each experimental plot (SV, RF, MC), dry soil samples were taken from the topsoil (0–2 cm), which is the exposed layer to wind erosion processes. A total of 48 samples ( $n = 16$ ; for each SV, RF, and MC soil type) were analyzed in the lab for soil properties using soil science methods (Klute, 1986; Rowell, 1994; Pansu and Gautheyrou, 2006) as follows.

Aggregate size distribution (ASD) was conducted by using the dry sieving method. The samples were placed on a set of six sieves in the diameters of 63–4000  $\mu\text{m}$  and were shaken in moderate amplitude for 8 min by an electronic sieving apparatus (RETSCH AS 300 Control). After sifting, every size fraction was weighted separately. In the fraction of  $>2000 \mu\text{m}$ , rock fragments were extracted from the rest of the soil particles. The results have been used to calculate the mean weight diameter (MWD) of the soil aggregates.

Particle size distribution (PSD) was performed by ANALYSETTE 22 MicroTec Plus laser diffractometer ([www.fritsch.com](http://www.fritsch.com)), which measures particles in the size range of 0.08–2000  $\mu\text{m}$ . The preparation of each sample includes splitting for replicate samples by a micro-splitter device and the removal of distinct organic matter. For the analysis, the replicates (100 mg) of each sample were dispersed in a Na-hexametaphosphate solution (0.5 %) and by sonication (38 kHz). PSD data was calculated using the Fraunhofer diffraction model. By using MasControl software, relevant parameters were determined statistically: mean size, median, and modes in multiple modal distributions, sorting values, size fraction weights. The size resolution for analyses was 1  $\mu\text{m}$ . The results allow the determination of the soil texture of sand (50–2000  $\mu\text{m}$ ), silt (2–50  $\mu\text{m}$ ), and clay ( $< 2 \mu\text{m}$ ) according to the USDA classification.

### Aeolian experiments

Aeolian experiments in the field were conducted in dry soils (Fig. 1) with a boundary-layer wind tunnel. Boundary-layer

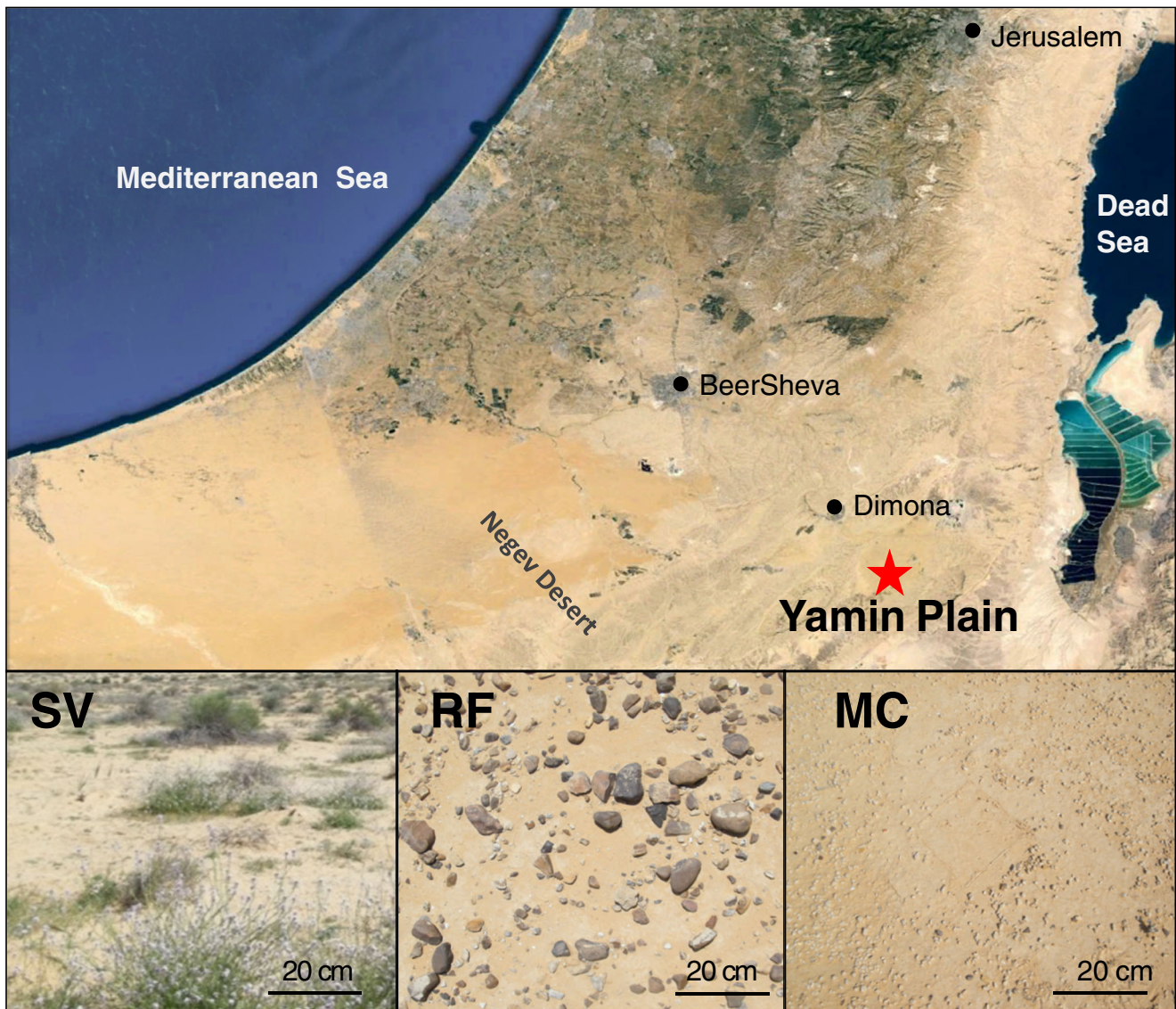


**Fig. 1** Location of the experimental plots (Yamin Plain) in the Negev, Israel, with the surface characteristics of sparse vegetation cover (*SV*), rock fragments (*RF*), and mechanical crust (*MC*)

wind tunnels enable aeolian simulations under standardized quasi-natural wind conditions (Shao, 2008) and provide quantitative information on aeolian particle transport, including sand fluxes (Katra et al., 2014) and dust emission rates from soils (Tanner et al., 2016). The wind tunnel used in this study has a cross sectional area in the order of  $0.5 \times 0.5$  m with open-floored working sections of up to 10 m length (see more details in Swet and Katra, 2016). The airflow in the tunnel is generated by an axial fan up to a maximum velocity of  $18 \text{ m s}^{-1}$ . Instruments installed in the test section of the tunnel enable quantification of wind characteristics and sediment transport.

The aeolian experiments in each plot were performed under two topsoil conditions: (1) natural surfaces (a non-disturbed topsoil) and (2) disturbed surface in which the topsoil was artificially disturbed at the upper 2 cm layer by the same

mechanical operation in all plots to simulate disaggregation of the topsoil. In each experimental plot, 12 sub-plots (replicas) were defined in size area of  $0.5 \text{ m} \times 10 \text{ m}$  in accordance with the dimensions of the experimental system. A total of 72 experiments were conducted in the field (3 plots, 2 soil treatments, 2 wind speeds, and 6 replicas).

The tunnel fan was set in two frequencies; the first of 32 Hz represents medium wind speed in the study area and above the threshold of particle transport ( $\sim 5 \text{ m s}^{-1}$ ), and the second of 44 Hz represents higher wind speed of typical aeolian erosion conditions in the studied area ( $\sim 9 \text{ m s}^{-1}$ ). In each experimental plot, the mean wind velocity profile was measured under both fan frequencies (32 and 44 Hz). The shear velocities ( $u_*$ ) calculated by the semi-empirical logarithmic law of Karman (Bagnold, 1941) were at the range of  $0.31\text{--}0.69 \text{ m s}^{-1}$ , depending on the fan frequency and the surface composition



(plot). During each test, the  $PM_{10}$  concentrations in the wind tunnel were measured by a particulate monitor (HAZ-DUST EPAM-5000, [www.skinc.com](http://www.skinc.com)). The EPAM-5000 uses light scattering technique to measure particle concentration and provide real-time data recordings at the range of 0.01 to 200  $mg\ m^{-3}$  (accuracy  $\pm 10\%$  to filter gravimetric test dust). The recorded  $PM_{10}$  data over time were converted into fluxes from the soil surface based on the wind tunnel dimensions and area of the experimental plot ( $3.75\ m^2$ ). The sand transport during the experiment was measured by a cylindrical piezo-electric sensor ([www.sensit.com](http://www.sensit.com)) that converts the impact energy of the saltating particles into electrical impulses. The Sensit data were logged as number of impact-particles (NP) on a Campbell Scientific Inc. CR-1000X data logger at 1 s intervals. The NP values were converted into horizontal saltator flux ( $mg\ m^{-2}\ s^{-1}$ ) considering the sensor impact area and the weight of the sand particles in the studied area at the size of 100–200  $\mu m$  (the mean weight of 1 particle = 57  $\mu g$ ). Each experiment lasted 400 s, representing a typical trend of soil erosion under limited sediment supply (Tanner et al., 2016).

## Results and discussion

### Topsoil characteristics

The PSD results show a tri-modal distribution in all the experimental plots (Fig. 2). The results represent both conditions of natural surface and disturbed surfaces – the samples were extracted prior to aeolian experiments in each condition, considering that no changes in PSD are expected in response to a short-term disturbance of the topsoil. SV soil was coarser, with significantly higher sand content than RF and MC soils. RF soil showed higher amount of clay compared to SV and MC soils. Differences in  $PM_{10}$  content in the soil were noted between the plots, in which the highest content was in MC plot while the lowest content in SV.

Aggregate size distribution was measured for each plot and soil conditions (natural and disturbed) (Fig. 3). In both soil conditions, the amount of aggregate at the size fraction of 250–500  $\mu m$  was higher compared with the other size fractions. The disturbance of the topsoil led to elimination of

aggregates  $>2000\ \mu m$  and to a reduction in the content of aggregates in the size fraction of 1000–2000  $\mu m$ . Accordingly, the amounts of the smaller size fractions 500–1000, 250–500, 125–250, 63–125, and  $<63\ \mu m$  were increased following disturbance by 18, 26, 34, 34, and 63 %, respectively. The most significant change occurred in MC plot with increased amount of the erodible fraction ( $< 500\ \mu m$ ) following disturbance.

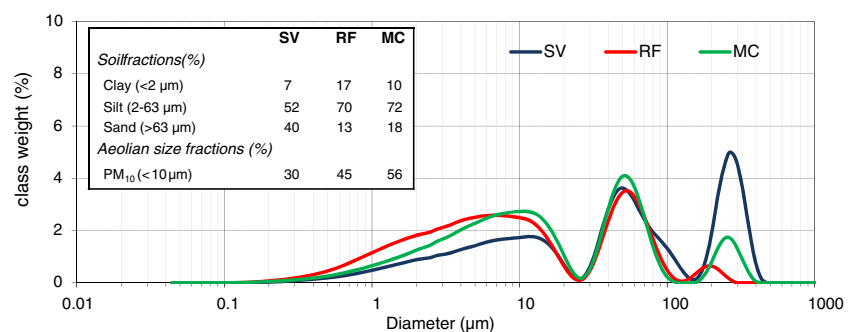
MWD driven from ASD was calculated for both conditions of natural and disturbed surfaces. The relatively low MWD values in natural condition in all plots (362.5, 512.5, and 433  $\mu m$  in SV, RF, and MC, respectively) indicate a potential of high susceptibility to wind erosion due to high proportion of erodible aggregate size fractions. The MWD values were lower at all experimental plots following disturbance of the natural surfaces (314.1, 283.2, and 253.3  $\mu m$  in SV, RF, and MC, respectively).

### Variations in $PM_{10}$ flux

The in situ aeolian experiments enabled the measurement of  $PM_{10}$  emission from the topsoil following wind erosion. A similar trend in  $PM_{10}$  emission was observed for natural and disturbed surfaces in both lower (32 Hz) and higher (44 Hz) wind velocities at all experimental plots (Fig. 4). The dust emission is characterized by increased  $PM_{10}$  concentrations in the first few seconds of the run up to a peak value, a relatively moderate decline followed by a steady-state phase which consist low  $PM_{10}$  concentrations. In all cases, increased wind velocity resulted in higher  $PM_{10}$  concentration over time (Fig. 3). At lower velocity (32 Hz frequency), the disturbance of the topsoil did not lead to a significant increase in  $PM_{10}$  concentrations at all plots. At high wind velocity (44 Hz frequency), significantly higher  $PM_{10}$  concentrations were recorded in all experiments. These changes particularly in the natural topsoil are indicative of the importance of wind velocity.

In order to estimate  $PM_{10}$  losses from the topsoils, the  $PM_{10}$  concentrations measured during the aeolian experiments were converted into  $PM_{10}$  fluxes from the soil ( $mg\ m^{-2}\ min^{-1}$ ) (Table 1). In all topsoil conditions and wind velocities, MC plot showed the highest  $PM_{10}$  flux (except for the disturbed

**Fig. 2** Average particle size distribution (PSD) by the laser diffractometer technique in the topsoils of sparse vegetation (SV), rock fragment (RF), and mechanical crust (MC). The size fractions derived from the PSD is presented in the box



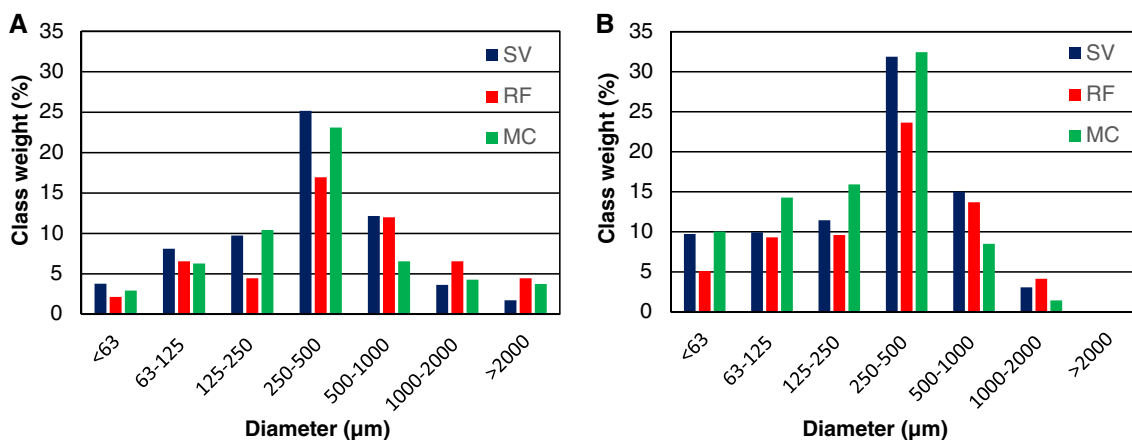


**Fig. 3** Aggregate size distribution (ASD) of SV, RF, and MC in natural (a) and disturbed (b) surface conditions

topsoil in frequency of 44 Hz) although with no statistical significance ( $p \leq 0.05$ ). Significant differences between the plots were noted only at disturbed topsoil in a 44 Hz frequency, were PM<sub>10</sub> flux from SV plot was significantly higher than RF plot. In both SV and MC plots, significantly higher PM<sub>10</sub> flux was obtained under 44 Hz in disturbed soil condition. RF plot showed no significant differences between the different topsoil conditions and wind velocities.

The PM<sub>10</sub> fluxes at the lower velocity (32 Hz frequency) were increased by 144.2 % in SV plot due to topsoil disturbance (Table 1). At the higher wind velocity (44 Hz frequency), the PM<sub>10</sub> fluxes were increased by 98.5–336.8 % in all plots. The results indicate that the effect of topsoil disturbance on PM<sub>10</sub> fluxes is stronger under higher wind velocities as demonstrated also by Li et al. (2015). However, the increase in wind velocity from 32 to 44 Hz in the natural topsoils led to

**Fig. 4** PM<sub>10</sub> concentrations measured during the aeolian experiments in SV, RF, and MC plots at 32 and 44 Hz frequencies and in natural and disturbed surface conditions

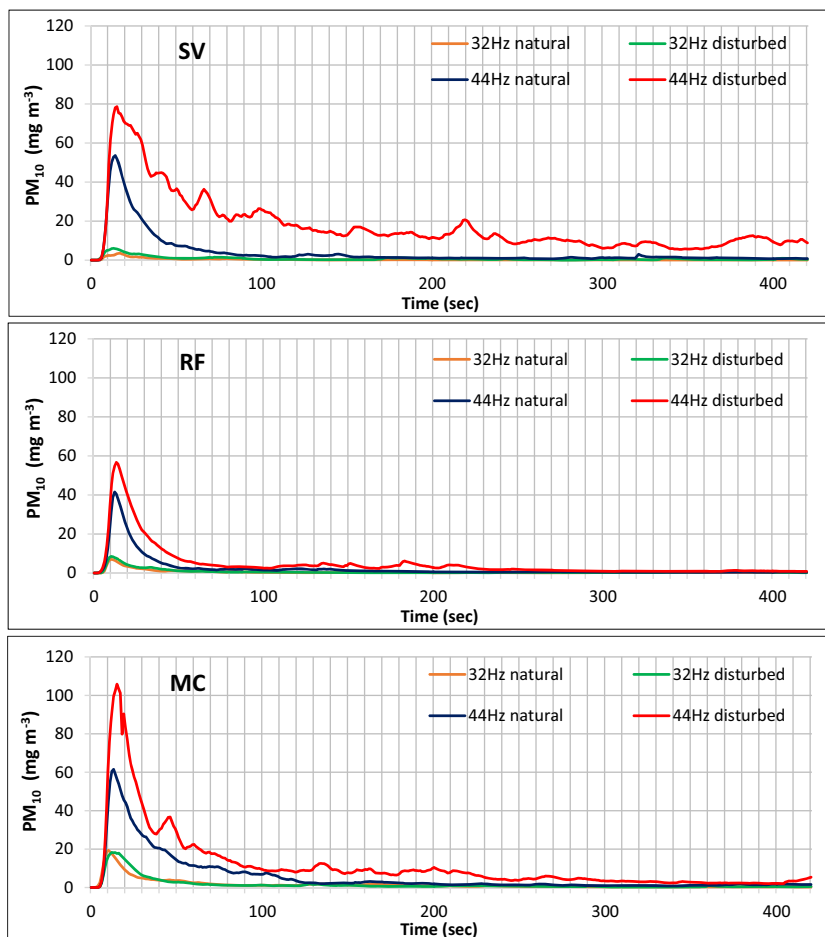


**Table 1** Average PM<sub>10</sub> flux from topsoil at SV, RF and MC in different fan frequencies and different topsoil conditions

Fan frequency		32 Hz (Wind velocity ~ 5 m s <sup>-1</sup> )			44 Hz (Wind velocity ~ 9 m s <sup>-1</sup> )		
Topsoil condition		Natural	Disturbed	Change (%)	Natural	Disturbed	Change (%)
PM <sub>10</sub> flux (mg m <sup>-2</sup> min <sup>-1</sup> )	<b>SV</b>	9.5 <sup>Aa</sup>	23.2 <sup>Aa</sup>	144.2	120.1 <sup>Aa</sup>	524.6 <sup>Ba</sup>	336.8
	<b>RF</b>	16.9 <sup>Aa</sup>	21.3 <sup>Aa</sup>	26.0	70.4 <sup>Aa</sup>	144.2 <sup>Ab</sup>	104.8
	<b>MC</b>	48.4 <sup>Aa</sup>	48.6 <sup>Aa</sup>	0.4	175.0 <sup>ABa</sup>	347.4 <sup>Bab</sup>	98.5

For each wind velocity, big letters represent differences in PM fluxes ( $p \leq 0.05$ ) between rows while small letters represent differences between columns. The change in the PM flux due to soil disturbance in each plot and wind velocity is presented in percentage

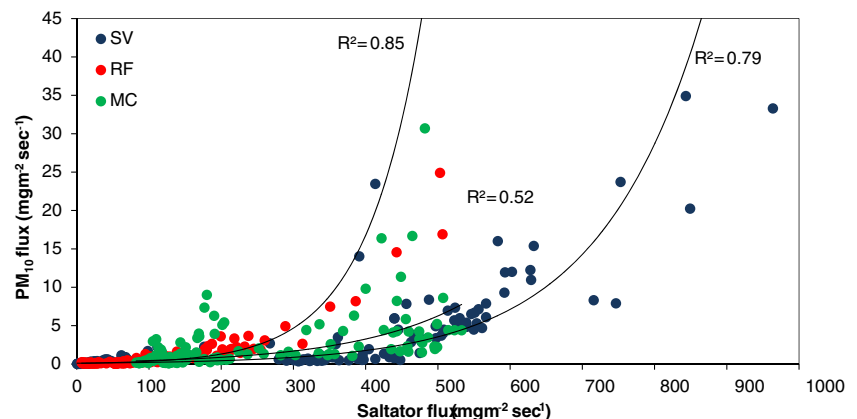
increase in PM<sub>10</sub> fluxes of 261.6 % (MC), 316.6 %, and 1164.2 % (SV). These changes are indicative of the importance of wind velocity in dust emission rates in the studied area. A positive linear correlation ( $R^2 = 0.73$ ) was found in the current study between the wind shear velocities ( $u_*$ ) and the PM<sub>10</sub> fluxes in the natural topsoils of all the plots. The correlation supports the findings of previous work (e.g., Sweeney and Mason, 2013).

### Impact of saltators

Dust particle is emitted from soils through physical mechanisms, including direct aerodynamic lifting, saltation bombardment and disaggregation/self-breakdown of saltating (sand-size) aggregates (Shao, 2008; Kok et al., 2012; Swet and Katra, 2016). The relationships between the soil saltators (i.e., sand particles and/or sand-sized aggregates) and PM<sub>10</sub> fluxes from the topsoil were examined. The results indicate an exponential correlation between the saltators and PM<sub>10</sub> emission in all soil compositions (Fig. 5). The strongest correlation was obtained in RF ( $R^2 = 0.84$ ) followed by SV ( $R^2 = 0.78$ ) and MC ( $R^2 = 0.52$ ). The higher content of soil PM<sub>10</sub> in MC plot compare to the other plots (Fig. 2) may contributed more to the total PM<sub>10</sub> fluxes via direct aerodynamic lifting mechanism rather than saltation bombardment and disaggregation, which can explain the weaker correlation to saltator flux obtained in this plot. In contrast, the significantly higher amount of sand particles in SV plot (Fig. 2) can be associated with the

highest PM<sub>10</sub> fluxes measured at the disturbed topsoil at 44 Hz (Table 1) through the saltation bombardment mechanism.

The saltation during the aeolian experiment was measured by the number of impact-particles (saltators) in the size range of ~80–500  $\mu\text{m}$  (in accordance with the wind threshold velocity used in this study). The impact-particles include not only loose sand particles but also sand-sized aggregates that participate in saltation. For a better understanding of PM<sub>10</sub> emission under soil aggregation, Pearson correlation coefficient between the amount of different aggregate sizes in the topsoil (based on ASD, Fig. 3) and PM<sub>10</sub> flux (Table 1) was examined. At the lower wind velocity (32 Hz), none of the aggregate size fractions were correlated with PM<sub>10</sub> fluxes. In order to transport aggregates, the wind needs to exceed a certain threshold velocity that depends on the size of the aggregate. The lack of correlation indicates that the wind at 32 Hz was below the threshold velocity even for the smallest aggregates (> 63  $\mu\text{m}$ ). Therefore, it is assumed that the PM<sub>10</sub> flux in this case is contributed mainly by the direct aerodynamic lifting mechanism. At higher wind velocity (44 Hz), relatively strong correlations were found between PM<sub>10</sub> fluxes and the amounts of aggregate at the sizes of <63  $\mu\text{m}$  ( $R_p = 0.89$ ,  $p < 0.05$ ) and 250–500  $\mu\text{m}$  ( $R_p = 0.87$ ,  $p < 0.05$ ). The correlation between PM<sub>10</sub> flux and the size fraction of <63  $\mu\text{m}$  can be explained by the fact that the particles smaller than 10  $\mu\text{m}$  are a part of the fraction of <63  $\mu\text{m}$ . The amplification of wind velocity (from 32 to 44 Hz) enabled the saltation of aggregates up to the size range of 500  $\mu\text{m}$  (Kok et al., 2012; Katra et al., 2014).

**Fig. 5** Dependence of PM<sub>10</sub> flux on saltators flux recorded for the different surface covers

Aggregates at this size range can enter saltation and release more PM<sub>10</sub> particles. Tisdall and Oades (1982) suggested that micro-aggregates (< 250 μm) can be easily eroded as a result of their small size, but on the other hand have higher internal strength than macro-aggregates (>250 μm) as a result of stronger bonds between the particles. The results of the correlation obtained for 250–500 μm aggregate size support this concept, enabling dust emission from aggregates by saltation bombardment and/or self-breakdown and disaggregation.

## Conclusions

Dust emission was examined in a study area with typical soil characteristics of arid dust sources. The results highlight variations in PM<sub>10</sub> emission due to surface compositions and topsoil disturbance. Surfaces with cover of sparse vegetation (SV) were found to be less resistant to aeolian wind erosion with the highest PM<sub>10</sub> fluxes compared to surfaces with cover of rock fragments (RF) cover and mechanical crust (MC). In all surfaces, the disturbance of the natural topsoil caused to decrease in the topsoil aggregation and increased PM<sub>10</sub> emission. The amount of loose PM<sub>10</sub> particles available at the surface for direct aerodynamic lifting and the amount of the less-stable aggregate size fractions (250–500 μm) are important factors for dust emission rates from these soils. The findings suggest that the specific aggregate size distribution of the soil is necessary for better estimation of PM<sub>10</sub> fluxes at the fine scale in arid soils. Calculations of the potential soil loess in this study highlight a direct impact of a short-term topsoil disaggregation on wind erosion. Dust deposition in the Negev, originates from different sources (such as Saharan dust storms) is about 150 g m<sup>-2</sup> per year, in which the PM<sub>10</sub> fraction is ~25 %. The high dust emission rates from disturbed soils in the Negev suggest a negative balance per year with significant reduction in topsoil PM<sub>10</sub> contents (Katra et al., 2016). A major consequence is related to reduction of clays and nutrients that play a key role in the soil stability and fertility in resource-limited ecosystems. The study findings have implications for modeling dust emission from source areas with complex surfaces, which are typical to many dust sources in deserts throughout the world.

**Acknowledgments** The study was supported by grants from the Israel Science Foundation (1100/11) and the Nuclear Research Center-Negev Israel.

## References

Al-Dousari AM, Al-Awadhi J (2012) Dust fallout in northern Kuwait, major sources and characteristics. *Kuwait Journal of Science and Engineering* 39(2 A):171–187

- Bacon SN, McDonald EV, Amit R, Enzel Y, Crouvi O, 2011. Total suspended particulate matter emissions at high friction velocities from desert landforms. *Journal of Geophysics Research*, 116, doi:10.1029/2011JF001965
- Baddock MC, Zobeck TM, Van Pelt RS, Fredrickson EL (2011) Dust emissions from undisturbed and disturbed, crusted playa surfaces: cattle trampling effects. *Aeolian Res* 3(1):31–41
- Bagnold RA (1941) *The physics of wind blown sand and desert dunes*. Methuen, London, 265
- Belnap J, Gillette D (1998) Vulnerability of desert biological soil crusts to wind erosion: the influences of crust development, soil texture, and disturbance. *J Arid Environ* 39:133–142
- Ganor E, Kronfeld J, Feldman HR, Rosenfeld A, Ilani S (2009) Environmental dust: a tool to study the patina of ancient artifacts. *J Arid Environ* 73(12):1170–1176
- Gillies JA, Nickling WG, King J (2006) Aeolian sediment transport through large patches of roughness in the atmospheric inertial sublayer. *J Geophys Res* 111:F02006. doi:10.1029/2005JF000434
- Hevia GG, Mendez M, Buschiazio DE (2007) Tillage affects soil aggregation parameters linked with wind erosion. *Geoderma* 140(1):90–96
- Hoffmann C, Funk R (2015) Diurnal changes of PM10-emission from arable soils in NE-Germany. *Aeolian Res* 17:117–127
- Katra I, Lancaster N (2008) Surface-sediment dynamics in a dust source from spaceborne multispectral thermal infrared data. *Remote Sens Environ*. doi:10.1016/j.rse.2008.03.016
- Katra I, Yizhaq H, Kok JF (2014) Mechanisms limiting the growth of aeolian megaripples. *Geophys Res Lett*. doi:10.1002/2013GL058665
- Katra I, Gross A, Swet N, Tanner S, Krasnov H, Angert A (2016) Substantial dust loss of bioavailable phosphorus from agricultural soils. *Scientific Reports* 6:24736
- King J, Nickling GW (2005) Representation of vegetation and other nonerodible elements in aeolian shear stress partitioning models for predicting transport threshold. *Journal of Geophysics Research* 110:F04015. doi:10.1029/2004JF000281
- Klute A (1986) *Methods of soil analysis. part 1. physical and mineralogical methods*. American Society of Agronomy, Inc
- Kok JF, Parteli EJ, Michaels TI, Karam DB (2012) The physics of wind-blown sand and dust. *Rep Prog Phys* 75(10):106901
- Krasnov H, Katra I, Koutrakis P, Friger M (2014) Contribution of dust storms to PM10 levels in an urban arid environment. *J Air Waste Manage Assoc* 64:89–94
- Langston G, McKenna Neuman C (2005) An experimental study on the susceptibility of crusted surfaces to wind erosion: a comparison of the strength properties of biotic and salt crusts. *Geomorphology* 72: 40–53
- Li F, Kang L, Zhang H, Zhao L, Shirato Y, Taniyama I (2005) Changes in intensity of wind erosion at different stages of degradation development in grasslands of Inner Mongolia, China. *J Arid Environ* 62(4): 567–585
- Li H, Tatarko J, Kucharski M, Dong Z (2015) PM<sub>2.5</sub> and PM<sub>10</sub> emissions from agricultural soils by wind erosion. *Aeolian Research*
- Pansu M, Gautheryrou J (2006) *Handbook of soil analysis: mineralogical, organic and inorganic methods* Springer
- Rowell DL (1994) *Soil science: methods and applications*. Longman Group Limited, Longman Scientific & Technical
- Shao Y (2008) *Physics and modelling of wind erosion* (Vol. 37). Springer Science & Business Media
- Shao Y, Raupach MR, Findlater PA (1993) Effect of saltation bombardment on the entrainment of dust by wind. *J Geophys Res* 98:12719–12726
- Sharratt B, Wendling L, Feng G (2010) Windblown dust affected by tillage intensity during summer fallow. *Aeolian Res* 2:129–134

- Singh P, Sharratt B, Schillinger WF (2012) Wind erosion PM<sub>10</sub> emission affected by tillage system in the world's driest rainfed wheat region. *Soil Tillage Res* 124:219–225
- Sweeney MR, Mason JA (2013) Mechanism of dust emission from Pleistocene loess deposits, Nebraska, USA. *J Geophys Res* 118: 1460–1471
- Sweeney MR, McDonald EV, Etyemezian V (2011) Quantifying dust emissions from desert landforms, eastern Mojave Desert, USA. *Geomorphology* 135:21–34
- Swet N, Katra I (2016) Reduction in soil aggregation in response to dust emission processes. *Geomorphology* 268:177–183
- Tanner S, Katra I, Haim A, Zaady E (2016) Short-term soil loss by aeolian erosion in response to conventional and organic agricultural practices. *Soil Tillage Res* 155:146–156
- Tisdall J, Oades J (1982) Organic matter and water-stable aggregates in soils. *J Soil Sci* 33(2):141–163
- Van Pelt RS, Baddock MC, Zobeck TM, Schlegel AJ, Vigil MF, Acosta Martinez V (2013) Field wind tunnel testing of two silt loam soils on the North America central high plains. *Aeolian Res* 10:53–59
- Vodonos A, Friger M, Katra I, Avnon L, Krasnov H, Koutrakis P, Schwatz J, Lior O, Novack V (2014) The impact of desert dust exposures on hospitalizations due to exacerbation of chronic obstructive pulmonary disease. *Air Quality, Atmosphere & Health* 7(4):433–439
- Wolfe SA, Nickling WG (1993) The protective role of sparse vegetation in wind erosion. *Prog Phys Geogr* 17:50–68
- Yitshak-Sade M, Novack V, Katra I, Gorodischer R, Tal A, Novack L (2015) Non-anthropogenic dust exposure and asthma medication purchase in children. *Eur Respir J* 45(3):652–660
- Zaady E, Katra I, Yizhaq H, Kinast S, Ashkenazy Y (2014) Inferring the impact of rainfall gradient on biocrusts' developmental stage and thus on soil physical structures in sand dunes. *Aeolian Res* 13:81–89